A Soft Optical Waveguide Coupled With Fiber Optics for Dynamic Pressure and Strain Sensing

Celeste To, Tess Hellebrekers, Jaewoong Jung, Sohee John Yoon, and Yong-Lae Park

***Abstract*—As the use of soft robotics and soft actuators becomes more popular, there is also an increased need for soft sensors that can perform robustly under various extreme conditions. While some applications find ultrathin flexible sensors sufficient, like electronic skin and wearable devices, there is still a critical need for robust sensing under extreme deformations. Previous work in highly stretchable sensing modalities commonly uses liquid conductors that couple a change in measured electrical resistance with applied stress. However, liquid conductors are expensive and difficult to encapsulate, leading to leakages that can damage machinery. As an alternative, this letter proposes an elastomeric waveguide coated with a thin reflective metallic layer that reflects internally propagating light. Upon deformation, microcracks in the reflective layer modulate the intensity of the light at the photodetector, leading to decrease in optical power. This letter describes the design, fabrication, and characterization of the proposed optical soft sensor. A prototype was created and characterized for pressure and strain up to 110 kPa and 30% strain, respectively.**

***Index Terms*—Soft sensors, fiber optics, waveguide, thin film coating.**

I. Introduction

THERE has been a large amount of interest and research in highly compliant sensors in the field of soft robotics. As progress is being made towards these types of robotic systems, there is a need for reliable sensing mechanisms that can interface and operate under extreme deformation. Electronic sensing skins and wearables have been a large research focus in the last decade, as shown in several review articles [1], [2]. Some of these technologies circumvent the problem by being extremely thin and flexible, but not necessarily stretchable. However, there are still applications where hyperelastic stretching is required. For this reason, soft and stretchable sensors have become a large topic of interest [3]–[5].

There are a variety of physical mechanisms that can be used for soft sensing. A large amount of effort has gone into developing and improving microfluidic sensors [6]–[9]. Such sensors commonly use eutectic gallium indium or galinstain in a polymeric microchannel where as deformation is applied, the change in resistance of the microfluidic substance can be related to the stress. This mechanism has been used in many soft strain gauges [10], [11] and pressure sensors [9], [10], [12]. Although microfluidic sensing is promising and conveniently couples stress with resistance, fabrication tends to be labor intensive and messy. Many researchers have considered alternative sensing mechanisms to avoid these drawbacks. Some have invented soft sensors which harness the power of magnetic fields [13]. In addition, optical power as a means of sensing has been a promising solution, with several optical soft sensors have been developed in the past ten years [14]–[19].

Conventionally, fiber Bragg gratings (FBGs) are used to detect several physical properties such as strain and temperature however they are too rigid with breaking points above 3% strain [20]. The idea of FBGs has also been utilized in several types of new soft sensors including soft pressure sensors [21], [22] and in tactile sensing arrays [23]. Recently we have proposed a highly stretchable optical sensor that can detect strain, pressure, and curvature [24]. It differs from the aforementioned sensors due to its large elongation at break. This sensor operates by having an optical power source shown through one end of the long transparent elastomeric structure, and on the other end there is a receiver. The exterior is coated with an inextensible reflective material similar to a slotted fiber optic cable [25]. Upon deformation, microcracks form to allow light to escape. We have shown successful results that relate this optical power loss with strain, pressure, and curvature. Although the device proved to work as intended, the form factor was larger than necessary due to embedded electronics in the structure, amongst other areas to improve upon.

In this letter, we have significantly improved upon the design, materials and fabrication process. We have miniaturized the structure by using plastic optical fibers and improved manufacturing methods, as shown in Figure 1. Fiber optic cables were used as a means of transmitting light from the power source to the photodetector, which are located remotely, instead of the previously embedded surface mount devices (SMDs). Compared

Manuscript received February 24, 2018; accepted June 22, 2018. Date of publication July 18, 2018; date of current version August 8, 2018. This letter was recommended for publication by Associate Editor A. Ferreira and Editor Y. Sun upon evaluation of the reviewers' comments. This work was supported in part by the Okawa Foundation Research Grant, in part by the National Research Foundation (NRF) funded by the Korean Government (MSIP) under Grant NRF-2016R1A5A1938472, and in part by the NAVER LABS Corporation. *(Corresponding author: Yong-Lae Park.)*

C. To is with the Department of Mechanical Engineering, Carnegie Mellon University, Pittsburgh, PA 15213 USA (e-mail: celeste.m.to@gmail.com).

T. Hellebrekers is with the Robotics Institute, Carnegie Mellon University, Pittsburgh, PA 15213 USA (e-mail: tessh@andrew.cmu.edu).

J. Jung and S. J. Yoon are with the Department of Mechanical and Aerospace Engineering, Soft Robotics Research Center, and the Institute of Advanced Machines and Design, Seoul National University, Seoul 08826, South Korea (e-mail: 7jaewoong7@naver.com; jylight@gmail.com).

Y.-L. Park is with the Robotics Institute, Carnegie Mellon University, Pittsburgh, PA 15213 USA, and also with the Department of Mechanical and Aerospace Engineering, Soft Robotics Research Center, and the Institute of Advanced Machines and Design, Seoul National University, Seoul 08826, South Korea (e-mail: ylpark@snu.ac.kr).

Digital Object Identifier 10.1109/LRA.2018.2856937

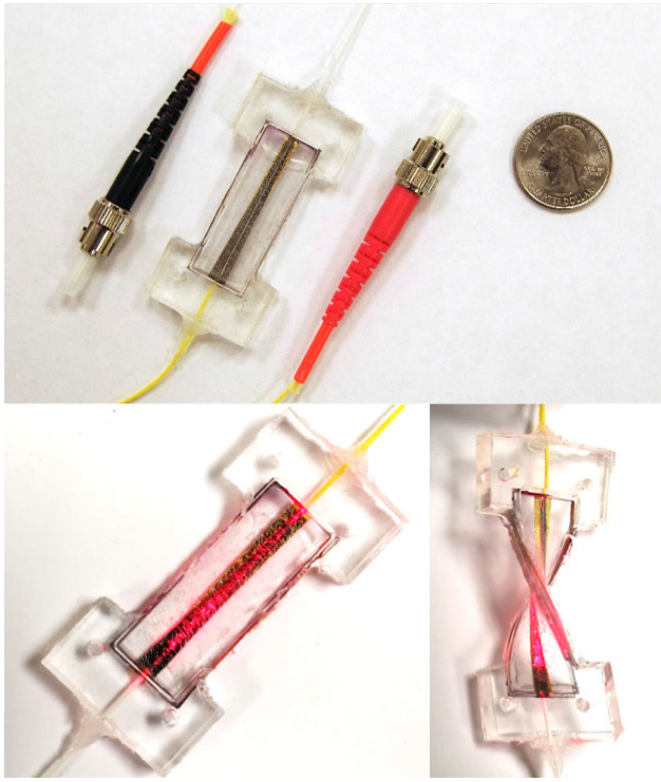

Figure 1. Complete optical soft sensor with fiber optic connectors (top), sensor prototype under approximately 10% strain (bottom-left), and twisting the soft sensor (bottom-right).

with previous designs, we are proposing use of optical fibers directly interfaced to the soft waveguide at the ends so that the internal structure remains free to stretch and deform. Additionally, sputter deposition was used for a controlled, uniform gold layer that can reflect the internally propagating light, which is a key difference from the optoelectronic soft sensor used in a soft prosthetic hand [26]. A simple model has been described to explain the mechanism behind the design and experimental results were obtained from this improved sensor. This type of sensor can be especially useful in medical devices due to its materials all being biocompatible, non-ferrous (non-magnetic), and non-chemical which makes it inert in medical environments. This letter describes the design, fabrication, and characterization of the aforementioned optical soft sensor.

II. Background

The mechanism behind this sensor can be explained through a simple model by directly relating the optical power loss to change in the waveguide surface area and Poisson's ratio of the sensor structure. Consider a cylindrical waveguide covered with an inextensible reflective metal layer (Figure 2-top). With no deformation applied, we can assume the metal layer and elastomer have a surface area of $2\pi r_o L_o$, where r_o is the original radius of the waveguide and L_o is the original length of the waveguide. Upon deformation, the surface area is defined as $2\pi rL$, where r and L are the current radius and length respectively. By rearranging Poisson's ratio of the material $\nu = -\varepsilon_r/\varepsilon_l$ where ε_r

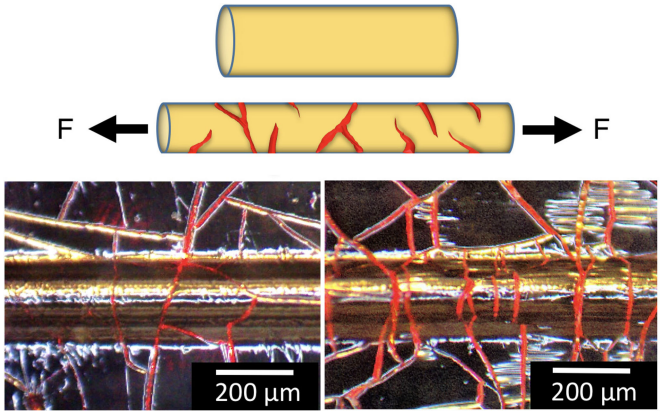

Figure 2. Conceptual drawing of microcrack formation upon deformation of an elastic waveguide (top) and microscopic images of an actual soft waveguide before (bottom-left) and after (bottom-right) being stretched.

and ε_l are the transverse and longitudinal strains of the sensor structure respectively, the relationship between radius and length is well defined:

$$\Delta r = -r_o \nu \frac{L - L_o}{L_o} \tag{1}$$

Assume that the inextensible layer completely reflects internally propagating light, and that the exposed elastomer allows for complete transmission. Then the change in signal depends on the ratio of the surface area of the inextensible layer to the total current surface area of the waveguide. Since the metal layer is inextensible, we can assume that its surface area remains the same regardless of sensor elongation. The ratio of the unchanging surface area of the metallic layer to the total surface area of the waveguide under elongation can be put in terms of the initial radius r_o, initial length L_o, Poisson's ratio ν of the elastomer, and the final length L:

$$\frac{SA_{gold}}{SA_{total}} = \frac{2\pi r_o L_o}{2\pi r L} = \frac{r_o L_o^2}{L(r_o L_o - \nu r_o L + \nu r_o L_o)} \tag{2}$$

It follows that we would expect optical power decay of this form as we stretch the sensor, which is shown in the experimental results. The ratio of optical power decay can be expressed by using equation (2), the ratio between surface areas:

$$\frac{P}{P_o} = \frac{r_o L_o^2}{L(C_1 - C_2 L)} \tag{3}$$

where $C_1 = r_o L_o + \nu r_o L_o$ and $C_2 = \nu r_o$ are constants dependent on the material properties and original size of the waveguide, P is the current optical power, and P_o is the optical power under no deformation.

III. Design

As mentioned there are already several optical sensing methods that exist for soft hyperelastic bodies. In particular, light modulation was used in pressure sensing using several methods [21], [22], [27]. We are using an alternative method by modulating light within our singular waveguide coupled with a reflective coating. The sensor functions by taking advantage

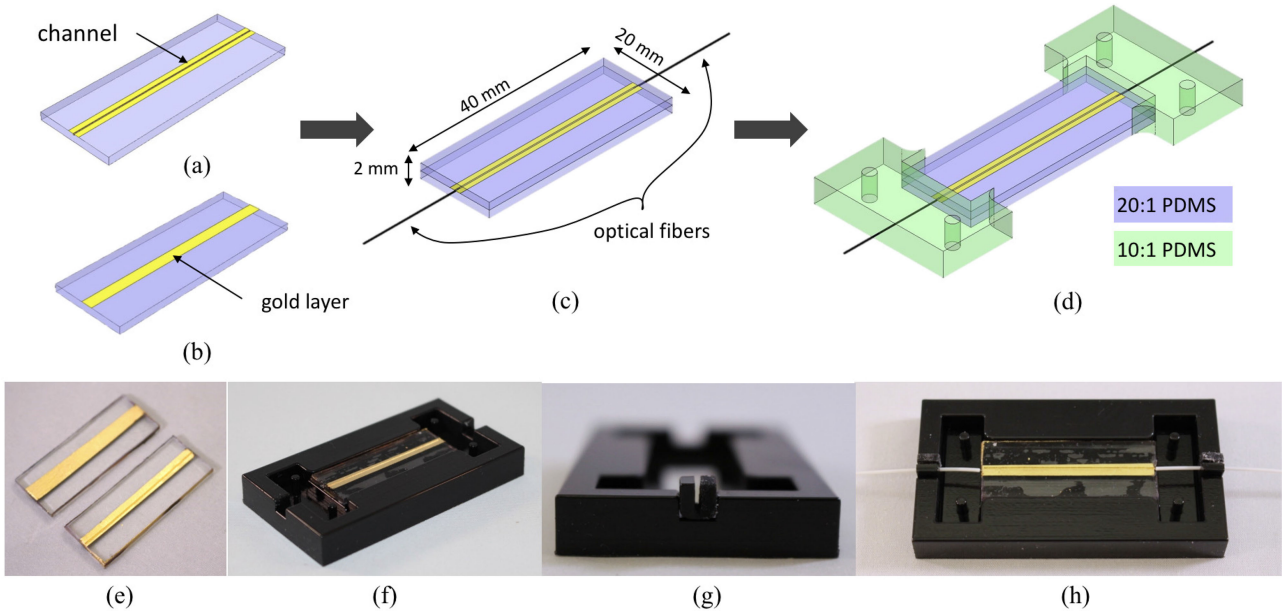

Figure 3. (a) Waveguide half with gold layered semi-circular channel and (b) half with flat gold layer are connected with to form (c) complete waveguide with inserted fiber optics. Finally, (d) two clamps are added for testing. (e) Two waveguide halves inserted into (f) mold for fiber alignment. (g) Close-up view of the fiber alignment pieces and (h) fibers inserted into place before clamps are poured.

of an inextensible reflective metal coating surrounding a completely elastic polymer waveguide which allows light to travel from one end to the other. Upon extension of the body, microcracks form along the metal coating - allowing the light to escape (Figure 2-bottom). The change in optical power from unperturbed to perturbed state can be measured and can be calibrated to measure the amount of deformation or force made to the sensor.

The sensor is composed of three main "components": optical fibers, elastomer, and metallic coating. At first glance the sensor has an I-beam, or "dog-bone," form. It consists of a polymeric semi-circle waveguide with the same polymeric material encasing the waveguide. The waveguide is semi-circular to make fabrication easier and the sensor less susceptible to misalignment. This housing and waveguide are both made from a 20:1 ratio polydimethylsiloxane (PDMS) to allow strains up to over 60%. The clamp ends have a 10:1 ratio of PDMS for ease of grasping onto during experimentation, as shown in Figure 3.

The reflective metal of choice here is gold (Au) due to its resistance to tarnishing and inert characteristic to bodily chemicals. Additionally a thin layer of titanium (Ti) was sputtered in conjunction with gold to help with adhesion between the gold layer and the elastomer. No titanium was used in early prototypes but the use of Ti in later prototypes has shown a significant improvement with wear. Since sputtering was used to build the layer in a semi-circle waveguide, excess Au was added to compensate for the almost vertical side walls. On one end of optical fibers there is a fiber optic emitter end using a high intensity infrared (IR) beam of 1490 nm. IR light is used because gold best reflects longer wavelengths (red to IR). On the other end, there is another fiber optic cable that acts as a receiver to measure optical power in micro-watts (μW). Both emitter and detector are built into the same device, an optical power meter (WaveTester, Optical Wavelength Laboratories). Using fiber optic cables ends allows for use in high-stretch environments where it is subjected to a great deal of deformation by avoiding unnecessary stress concentrations. In addition, the optical and electronic units are clear from the area of dynamic forces.

The selection of materials was made with the intent that we could implement this sensor in medical related devices that would come in contact with humans. For example, gold does not react inside or outside the human body, which is why it is commonly used in the medical field. Titanium is also biocompatible as it is commonly used in prosthetic implants. Lastly, PDMS is commonly used in current medical devices because it is easy to sterilize, high permeability, and biocompatibility.

IV. Fabrication

All molds were printed as negative images of the desired shape using an Objet30 with VeroBlack material. All elastomer preparation steps included degassing to improve structural integrity and remove air bubbles and curing for 4 hours at 60 °C in an oven.

First, two rectangular halves using a 20:1 ratio of PDMS (Sylgard 184, Dow Corning) are made in preparation for the internal waveguide. The top half is 1 mm $\times$ 20 mm $\times$ 40 mm, while the bottom half is 1.5 mm $\times$ 20 mm $\times$ 40 mm with a semi-circular channel (d $=$ 0.22 mm) spanning the length of the sample (Figure 3-a). 5 mm $\times$ 40 mm Kapton tape masks are applied to the edges of these rectangular halves to leave a 10 mm $\times$ 40 mm exposed area in the center. Then, the samples are sputtered with 100 nm of titanium to improve adhesion of the 300 nm of gold layer. Afterwards the mask is removed to

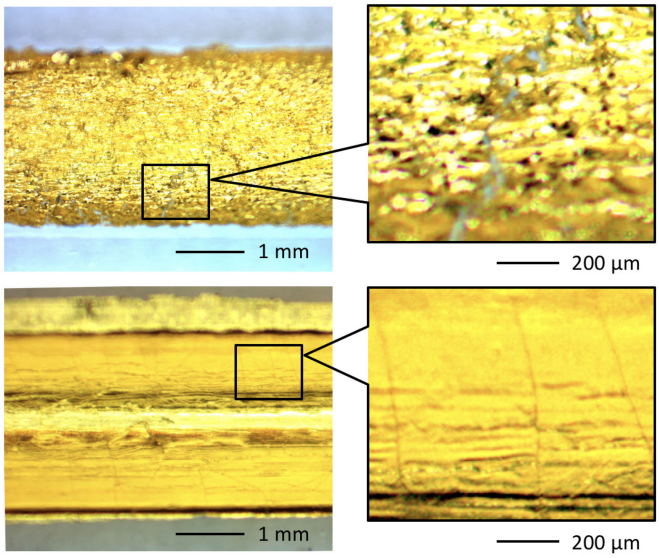

Figure 4. Example of gold-layer coatings on semicylindrical PDMS waveguides made by gold-leaf (top) and sputtering (bottom) methods for comparison. The magnified views on the right side shows initial microcracks before stretching. While the gold leaf coating shows many wrinkles with relatively large initial cracks, the sputtered coating shows a uniformly coated layer with only hairline initial cracks.

show only the area where the waveguide will be formed with the reflective Au layer (Figures 3-a and 3-b). The semi-circular channel is placed with the channel upward in another mold with room to add the fiber optic cables. An optical fiber ($\phi = 250\ \mu$m) is stripped to remove the polymer protective coating until the bare fiber cladding ($\phi = 125\ \mu$m) is exposed. Using fiber alignment pieces in the mold, they are lined up in the semi-circular waveguide where there is very little clearance between the fiber and the wall to ensure an effective signal response. Then more 20:1 elastomer is poured over the channel, covered with transparency film to flatten the surface, and cured in the oven. In order to finish the internal waveguide, more 20:1 elastomer is spin coated on top of the channel half and the other previously prepared rectangular half is attached with the reflective layer facing down (Figure 3-c). This completely encloses the waveguide to create a completely reflective interior for the light to pass through. The final waveguide housing, 2 mm $\times$ 20 mm $\times$ 40 mm (depth, width, and length, respectively), is relatively large compared to protect the internal waveguide and make the sensor durable. After that part is fully cured, the 10:1 elastomer (Sylgard 184, Dow Corning) is poured to create the clamps at either end of the sensor (Figure 3-d). The ends overlap 5 mm of each side to give the sensor an effective length of 30 mm. Once the sensor is complete, silicone adhesive (Sil-Poxy, Smooth-On) is added to the fiber optic cable junction to secure the connection.

The sputtering method proposed in this work significantly improved the quality of the reflective gold layer on the waveguide compared to the previous gold leaf method [24]. The gold layer made by sputtering was not only more uniform but also contains much smaller and less initial microcracks before stretching, as shown in Figure 4.

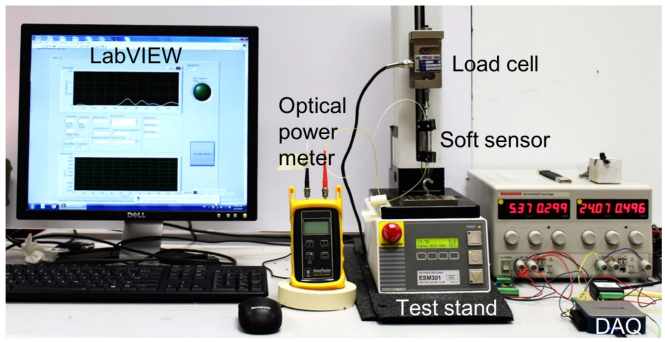

Figure 5. Overall test setup with soft sensor, optical power meter, load cell as reference, motorized test stand, DAQ board, and LabVIEW monitor.

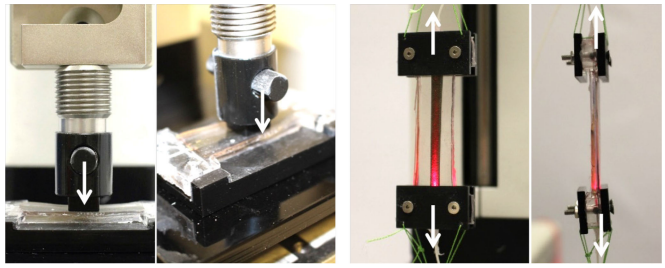

Figure 6. Front and side views of test setup with motorized test stand for pressure (left) and strain (right) testing, respectively.

V. Results

Stress-strain and failure tests were performed to characterize the mechanical properties of the sensor. In addition, pressure and strain tests were performed to characterize the optical signal using a motorized material test stand (ESM301, Mark-10) and a single-axis load cell (STL-50, AmCells), as shown in Figure 5. The detailed test setups for pressure and strain testing is shown in Figure 6. While the optical signals from the soft sensor were measured using the WaveTester at a sampling rate of 1 Hz, the displacement and the applied pressure were measured by the encoder in the test stand and the load cell, respectively. The raw signal from the load cell was acquired through a data acquisition (DAQ) device (USB-6000, National Instruments) and recorded by a DAQ software package (LabVIEW, National Instruments). A band pass filter (0.5–5 Hz) and a minimum-phase equiripple finite impulse response (FIR) filter were applied to all of the following raw signals (Figure 7).

A. Elastomer Response

Three sensors were loaded until failure to determine max strain for further testing. Results showed failure at 65, 50, and 20% strain for 10 mm/min, 5 mm/min, and 1 mm/min, respectively. Subsequent strain tests were designed to fall well within this window. As expected, the elastomer shows slight variation in max strain due to the viscoelastic properties of the elastomer, especially at different speeds.

For the stress-strain curve, the sensor was loaded axially between two clamps up to 33% strain at a rate of 5 mm/min. The gauge length was measured at the start of each test to calculate

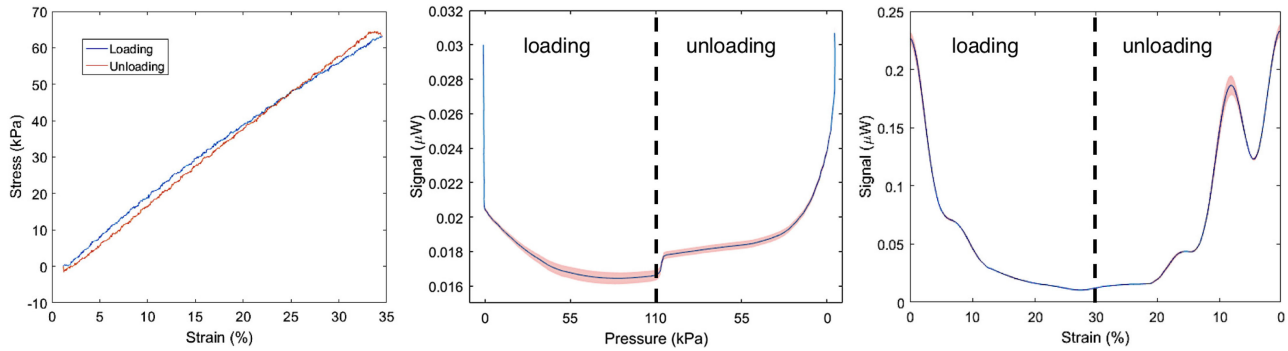

Figure 7. Experimental results of stress-strain response for the sensor up to 33% strain (left), signal-pressure response up to 110 kPa (middle), and signal-strain response up to 30% strain (right).

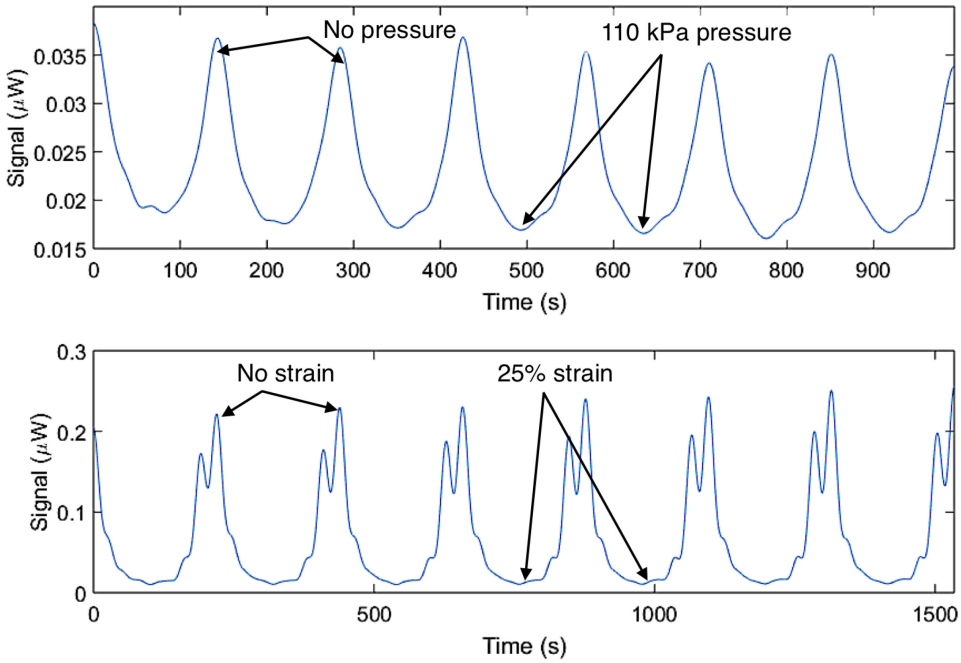

Figure 8. Subsets of cyclic test results for pressure at 1 mm/min (top) and strain at 5 mm/min (bottom) for 30 cycles each.

engineering strain. Engineering stress was calculated with the known cross-sectional area of each sample and the force data measured at 250 Hz using the load cell. A maximum stress of approximately 60 kPa was observed. Minimal hysteresis was shown between loading and unloading (Figure 7-left).

B. Pressure Response

A custom test stand and square indenter was built to ensure even and complete distribution of pressure (Figure 6-left). Force was applied to the middle of the waveguide to a depth of 1 mm at a rate of 1 mm/min. The load cell collected force data at 250 Hz, while the WaveTester collected optical power data at 1 Hz. The relationship between signal response and applied pressure is shown in Figure 7-middle. During unloading, the elastomer exhibits hysteresis, resulting in a bias around 110 kPa.

The pressure response was also recorded to a depth of 1 mm at 1 mm/min for 30 cycles to confirm robustness of the signal. Pressure sensitivity was estimated to be 3.5e–5 μW/kPa. A representative subset of cycles are shown in Figure 8-top. Overall, the signal is very repeatable over time, despite the elastomeric properties. However, the resting signal appears to be decreasing slightly over time. We attribute this drift largely due to the viscoelasticity of the base polymer and not the gradual degradation of the gold coating, as it is completely encapsulated by polymer. Similarly, when the motor changes direction between loading and unloading, there is a slight perturbation we attribute to the movement of the testing stand. Immediately after unloading the closed channel, there is a delayed signal response we attribute to hysteresis of the elastomer.

C. Strain Response

For all strain testing, the sensor was suspended between two hooks, attached by custom printed clamps to distribute stress along the dog-bone sample evenly (Figure 6-right). Each test was inspected to ensure proper alignment and a pre-strain of 3%. Gauge length was measured to calculate engineering strain.

The optical power, in μW, was measured at 1 Hz using the WaveTester. The sensor was loaded up to 30% strain at a rate of 5 mm/min. The loading and unloading signals are shown in Figure 7-right. Due to the hysteretic behavior of the polymer material, the fibers may become temporarily misaligned while unloading stress and results in a local convex region.

In addition, this strain test was performed for 30 cycles at 5 mm/min, up to a strain of 25%. Strain sensitivity was estimated to be 2.5e–4 μW/mm. A representative subset of cycles are shown in Figure 8-bottom, and appear consistent over time. However due to fiber movement during testing, there are notable discrepancies in the curves, especially between cycles. We believe this is due to the motor changing directions, causing perturbations in the testing stand, and fiber misalignment. However, the signal changes predictably in spite of small manufacturing disparities. During the cyclic test there is a noticeable decrease in signal during unloading. We believe this is due to fiber movement and misalignment while the test stand unloads the strain.

VI. Application

To demonstrate an example of applications of the proposed sensor, one of the prototypes was installed to a commercial six degrees-of-freedom (DOF) robotic arm (UR3, Universal Robots) and tested for repeated dynamic force sensing. The optical soft sensor was attached to the end-effector of the robotic arm (Figure 9-top) and compressed and released by the indenter attached to a commercial load cell (RFT60-HA01, ROBOTOUS) by moving the end-effector vertically at a constant rate of 5 mm/sec. The displacement of the end-effector, the force measured by the load cell, and the output from the soft sensor were plotted (Figure 9-middle). The result showed repeatable force response with a hysteresis loop (Figure 9-bottom). The hysteresis was mainly from the low sensitivity of the soft sensor in the low force range and the delay in restoring the original shape of the sensor when the load was removed.

VII. Discussion and Future Work

We presented a soft optical sensor alternative to liquid metal soft sensors. While the fabrication process is simple, small human errors in fiber alignment, elastomer mixing, and gold sputtering can lead to disparities between sensors. For this reason, we have highlighted strain and pressure responses from the same sensor, although we tested many sensors from different fabrication batches. Despite the signal noise, pressure and strain response have been shown to be repeatable. While we introduced 10:1 PDMS clamps and silicone adhesive to restrict fiber movement, we expect further fabrication improvements to control fiber alignment would improve the signal patterns. We also plan to design our own circuitry to collect optical intensity data at a sampling rate of 250 Hz and explore hybrid elastomer alternatives to improve the working strain range to approximately 100%.

Beyond manufacturing improvements, designs with a deterministic architecture could regulate the formation of microcracks in the gold coating. One example would be making the waveguide with alternating soft and rigid regions completely covered with gold. This would cause most of the light loss to occur at the soft regions with high stress concentrations. Alternatively, we could limit the gold coating to the soft regions to maximize the optical power loss for increased sensitivity.

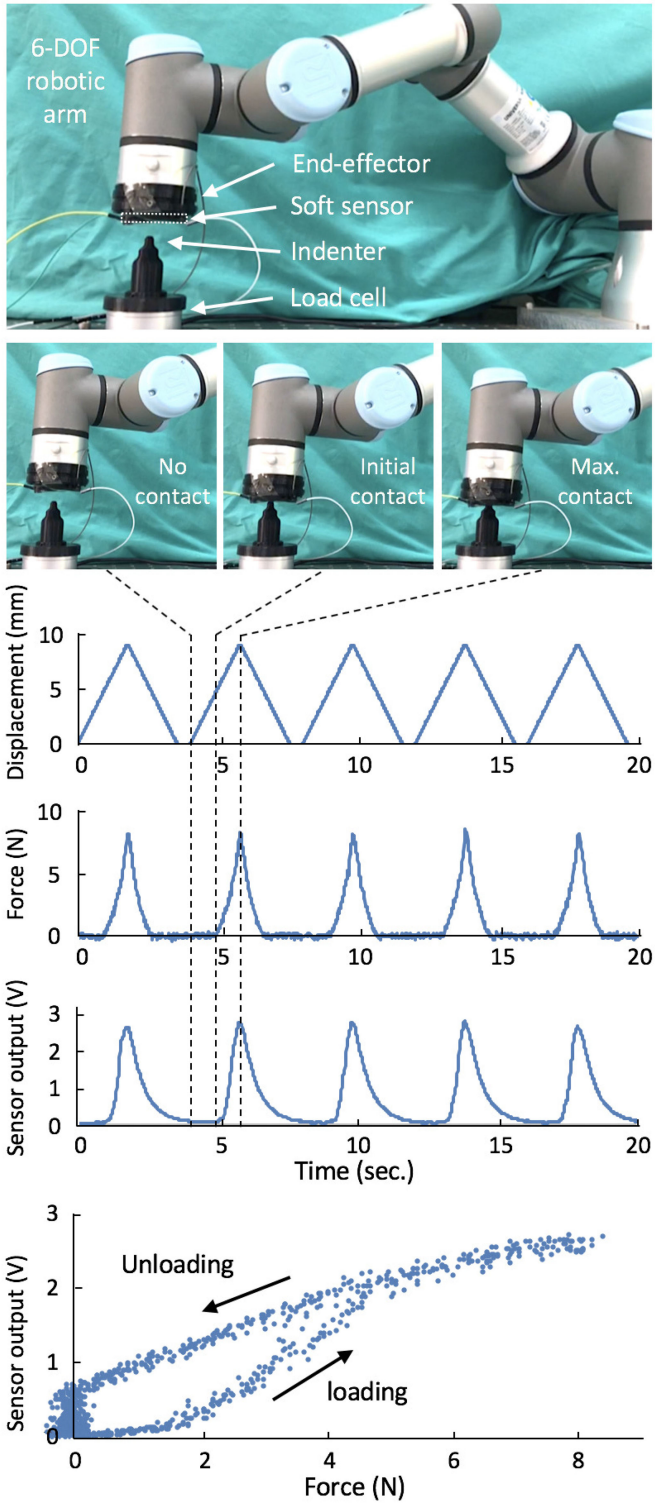

Figure 9. Experimental setup (top) and results of end-effector displacement, applied force, and sensor output (middle) for dynamic loading and unloading test and relationship between sensor output and applied force (bottom).

We also plan to investigate modified geometry to allow the sensor to respond to multiple modes of deformation simultaneously (i.e. multi-modal sensing) by combining multiple sensing elements in one sensor. This would be particularly valuable for robotic applications, like joint angle sensing, that often require 3- to 6-axis capabilities.

VIII. Conclusion

In review, a soft waveguide with embedded fiber optics was designed, fabricated, and characterized. We reported signals for pressure up to approximately 110 kPa and strain up to 30%. It was shown to be repeatable over time, with minimal hysteresis. Some key advantages are simplified the fabrication process, the simple electronic interface, and the small form factor. This sensor further demonstrates the potential for optics in soft sensing.

References

[1] M. L. Hammock, A. Chortos, B. C. K. Tee, J. B. H. Tok, and Z. Bao, "25th anniversary article: The evolution of electronic skin (E-Skin): A brief history, design considerations, and recent progress," *Adv. Mater.*, vol. 25, no. 42, pp. 5997–6038, 2013.

[2] P. B. Shull and D. D. Damian, "Haptic wearables as sensory replacement, sensory augmentation and trainer—A review," *J. NeuroEng. Rehabil.*, vol. 12, no. 1, pp. 59-1–59-13, 2015.

[3] T. Lu, L. Finkenauer, J. Wissman, and C. Majidi, "Rapid prototyping for soft-matter electronics," *Adv. Funct. Mater.*, vol. 24, no. 22, pp. 3351–3356, 2014.

[4] M. Amjadi, K. U. Kyung, I. Park, and M. Sitti, "Stretchable, skin-mountable, and wearable strain sensors and their potential applications: A review," *Adv. Funct. Mater.*, vol. 26, no. 11, pp. 1678–1698, 2016.

[5] C. Majidi, "Soft robotics: A perspective—Current trends and prospects for the future," *Soft Robot.*, vol. 1, no. 1, pp. 5–11, 2014.

[6] J.-B. Chossat, H.-S. Shin, Y.-L. Park, and V. Duchaine, "Soft tactile skin using an embedded ionic liquid and tomographic imaging," *J. Mech. Robot.*, vol. 7, no. 2, 2014, Art. no. 021008.

[7] D. M. Vogt, Y.-L. Park, and R. J. Wood, "Design and characterization of a soft multi-axis force sensor using embedded microfluidic channels," *IEEE Sensors J.*, vol. 13, no. 10, pp. 4056–4064, Oct. 2013.

[8] C.-Y. Wu, W.-H. Liao, and Y.-C. Tung, "Integrated ionic liquid-based electrofluidic circuits for pressure sensing within polydimethylsiloxane microfluidic systems," *Lab Chip*, vol. 11, no. 10, pp. 1740–1746, 2011.

[9] R. D. Ponce Wong , J. D. Posner, and V. J. Santos, "Flexible microfluidic normal force sensor skin for tactile feedback," *Sensors Actuators A, Phys.*, vol. 179, pp. 62–69, 2012.

[10] Y.-L. Park, C. Majidi, R. Kramer, P. Bérard, and R. J. Wood, "Hyperelastic pressure sensing with a liquid-embedded elastomer," *J. Micromech. Microeng.*, vol. 20, 2010, Art. no. 125029.

[11] Y.-L. Park, B.-R. Chen, and R. J. Wood, "Soft artificial skin with multi-modal sensing capability using embedded liquid conductors," in *Proc. IEEE Sensors Conf.*, Limerick, U.K., Oct. 2011, pp. 81–84.

[12] Y.-L. Park, B. R. Chen, and R. J. Wood, "Design and fabrication of soft artificial skin using embedded microchannels and liquid conductors," *IEEE Sensors J.*, vol. 12, no. 8, pp. 2711–2718, Aug. 2012.

[13] S. Ozel, N. A. Keskin, D. Khea, and C. D. Onal, "A precise embedded curvature sensor module for soft-bodied robots," *Sensors Actuators A, Phys.*, vol. 236, pp. 349–356, 2015.

[14] Z. F. Zhang, X. M. Tao, H. P. Zhang, and B. Zhu, "Soft fiber optic sensors for precision measurement of shear stress and pressure," *IEEE Sensors J.*, vol. 13, no. 5, pp. 1478–1482, May 2013.

[15] D. Cai, A. Neyer, R. Kuckuk, and H. Heise, "Optical absorption in transparent PDMS materials applied for multimode waveguides fabrication," *Opt. Mater.*, vol. 30, no. 7, pp. 1157–1161, Mar. 2008.

[16] P. Kampmann and F. Kirchner, "Integration of fiber-optic sensor arrays into a multi-modal tactile sensor processing system for robotic end-effectors," *Sensors*, vol. 14, no. 4, pp. 6854–6876, Jan. 2014.

[17] S. Kopetz, D. Cai, E. Rabe, and A. Neyer, "PDMS-based optical waveguide layer for integration in electrical–optical circuit boards," *AEU—Int. J. Electron. Commun.*, vol. 61, no. 3, pp. 163–167, Mar. 2007.

[18] P. Polygerinos, L. D. Seneviratne, R. Razavi, T. Schaeffter, and K. Althoefer, "Triaxial catheter-tip force sensor for MRI-guided cardiac procedures," *IEEE/ASME Trans. Mechatronics*, vol. 18, no. 1, pp. 386–396, Feb. 2013.

[19] C. Larson *et al.*, "Highly stretchable electroluminescent skin for optical signaling and tactile sensing," *Science*, vol. 351, no. 6277, pp. 1071–1074, 2016.

[20] V. Chean, E. Robin, R. E. Abdi, and J.-C. Sangleboeuf, "Study of the mechanical behavior of the optical fiber by a mark-tracking method," in *Proc. EPJ Web Conf.*, 2010, vol. 6, Art. no. 34002.

[21] S. Yun *et al.*, "Polymer-waveguide-based flexible tactile sensor array for dynamic response," *Adv. Mater.*, vol. 26, pp. 4474–4480, 2014.

[22] M. Ramuz, B. C.-K. Tee, J. B.-H. Tok, and Z. Bao, "Transparent, optical, pressure-sensitive artificial skin for large-area stretchable electronics," *Adv. Mater.*, vol. 24, no. 24, pp. 3223–3227, Jun. 2012.

[23] J.-S. Heo, J.-H. Chung, and J.-J. Lee, "Tactile sensor arrays using fiber Bragg grating sensors," *Sensors Actuators A, Phys.*, vol. 126, no. 2, pp. 312–327, 2006.

[24] C. To, T. L. Hellebrekers, and Y. L. Park, "Highly stretchable optical sensors for pressure, strain, and curvature measurement," in *Proc. IEEE/RSJ Int. Conf. Intell. Robot. Syst.*, Hamburg, Germany, Sep. 2015, pp. 5898–5903.

[25] S. C. Ryu, Z. F. Quek, P. Renaud, R. J. Black, B. L. Daniel, and M. R. Cutkosky, "An optical actuation system and curvature sensor for a MR-compatible active needle," in *Proc. IEEE Int. Conf. Robot. Automat.*, Saint Paul, MN, USA, May 2012, pp. 1589–1594.

[26] H. Zhao, K. O'Brien, S. Li, and R. F. Shepherd, "Optoelectronically innervated soft prosthetic hand via stretchable optical waveguides," *Sci. Robot.*, vol. 1, no. 1, 2016, Art. no. eaai7529.

[27] G. Kodl, "A new optical waveguide pressure sensor using evanescent field," in *Proc. 54th Electron. Compon. Technol. Conf.*, Las Vegas, NV, USA, Jun. 2004, pp. 1943–1946.